IIETA International Information and Engineering Technology Association
Advancing the World of Information and Engineering

Annales de Chimie - Science des Matériaux
Vol. 49, No. 6, December, 2025, pp. 615-625
Journal homepage: http://iieta.org/journals/acsm

Evaluation of Experimental Results of GFRP-Confined Concrete and Existing Stress-Strain Models

Leila Hamzaoui*, Khadidja Sekhri, Djarir Yahyaoui, Abdelhakim Zendaoui

Civil Engineering Laboratory – Risks and Structures in Interactions (LGC-ROI), Department of Civil Engineering, Faculty of Technology, University of Batna 2 – Mostefa Ben Boulaïd, Batna 05000, Algeria

Corresponding Author Email: l.hamzaoui@univ-batna2.dz

https://doi.org/10.18280/acsm.490604

Received: 18 November 2025
Revised: 19 December 2025
Accepted: 25 December 2025
Available online: 31 December 2025

Keywords:
confined concrete, fiber–reinforced polymer, glass fiber, axial compression, stress-strain model

ABSTRACT

This study investigates the enhancement of mechanical properties in glass fiber-reinforced polymer (GFRP) concrete confined with fiber reinforced polymer (FRP). Experimental tests were conducted on confined circular concrete samples with varying strengths and glass fiber contents. The axial compression behavior was analyzed by examining the stress-strain (σ-ε) relationship. Due to the wide range of predictive models available, selecting an accurate expression to represent the (σ-ε) behavior for validating experimental results is challenging. To address this, six numerical programs were developed based on six behavioral models from previous research deemed effective. These models were compared against experimental data from samples differing in strength, fiber content, and number of confinement layers. The findings emphasize the relevance and accuracy of certain tested formulations. However, some models, despite their strong research background, tend to either underestimate or overestimate the compression response, limiting their reliability for design and prediction purposes.

1. INTRODUCTION

Glass fiber-reinforced polymer (GFRP) is a promising alternative to traditional construction methods. The fibers act as reinforcement, increasing the tensile strength and improving the flexibility of the concrete. In addition, to optimize the behavior of concrete in compression, the use of technologies based on fiber reinforced polymer (FRP) as a containment device represents an innovative and effective solution. The combination of these materials makes it possible to produce a material that is both lightweight, durable and offers increased tensile and compression performance. Glass fibers stand out as an economical option with commendable mechanical properties suitable for many construction tasks.

Fiber-reinforced concrete appeared in the 1970s; the FPR was designed to improve the overall performance of concrete structures, during its years the behavior of concrete elements confined by polymer fibers under axial loading has been widely studied [1-6], and recently [7, 8].

Several researchers have suggested analytical and numerical models in order to predict the behavior of ordinary concrete confined by polymer fibers in the face of a concentrated static load [9-17]. Nevertheless, the potential of these constituent models to predict the stress-deformation relationship (σ-ε) of composite and confined concrete elements is often little explored. Moreover, it is particularly difficult to compare the experimental results with a simple and reliable theoretical model; despite the abundance of existing studies (The current analysis has highlighted various discrepancies between these studies). Indeed, this research highlights an experimental study carried out at the Civil Engineering Laboratory of the University of Batna2. The following sections detail this experimental approach: The first section is dedicated to the study of the experimental behavior of reinforced and confined cylinders with GFRP subjected to a monotonous compression load. We summarize, discuss and compare the experimental results in order to highlight the key parameters of the components that have a significant impact on the mechanical behavior of composite parts. In addition, we quantify the advantage of this new design compared to unconfined reference specimens.

In the second section, an analysis that addresses six behavioral laws suggested by the literature is examined in order to compare the experimental results with the theoretical models of various original formulations. According to a study of the literature, we have found that there are several formulations that describe the behavior of concrete confined by GRFP depending on various factors and parameters. This complicates the choice for any researcher wishing to select the most appropriate expression that accurately and accurately reflects this behavior. In this study, our attention will be specifically focused on this point. This study will focus on this specific aspect; based on our experimental results, we will perform a comparative analysis with various models suggested in previous research; this comparison will allow us to identify and distinguish the most suitable analytical model to explain the relationship (σ-ε). The performance of the proposed containment model and those existing in the literature was evaluated using the database collected in this study, which aimed to provide a reference to predict the behavior of

concrete containing glass fibers wrapped in a FRP jacket.

2. EXPERIMENTAL TESTS

2.1 Sample preparation and configuration

The preparation and arrangement of the specimens for the experimental investigation on GFRP were carried out with great precision in order to guarantee reliable test results. A range of specimen types was used (36 specimens), cylindrical specimens. The specimens were manufactured with a diameter of 150 mm and a height of 300 mm, the physical properties are summarized in Table 1.

Table 1. The physical properties of concrete

Concrete Specimens	S8.5	S16	S25
Concrete Compressive strength (MPa)	8 .5	16	25
Cement (kn.m^{-3})	200	300	400
Sand (kn.m-^{3})	853	810	773
Aggregate (kn.m^{-3})	481/853	520	496
Water (kg.m^{-3})	100	132	193
superplasticiser	As required		

These specimens have been carefully configured to evaluate the performance of the GFRP under axial compression. Glass fibers were integrated into the concrete matrix using a bidirectional local fiberglass and polyester resin jacket technique, which was used to develop a low-cost GFRP confinement (this category is the most used). Layers (1, 2 and 3 layers) enveloped the concrete specimens which in turn contained alkali–resistant glass fibers in order to control cracks and improve the toughness of the mixture. The proportion of glass fibers relative to concrete was systematically maintained at specific ratios according to different percentages (0, 0.3, 0.6, 0.9 and 1.2%) by volume in order to know the appropriate ratio in order to predict the structural performance while preserving the compressive integrity. All the characteristics of glass fiber reinforcing polymers, whether they are used as fibers in concrete paste or as a containment jacket, are available in Table 2.

Table 2. The characteristics of the GFRP

	Alkali-Resistant	GFRP	Epoxy Resin
Density(kg.m^{-3})	2600	-	-
Length /diameter (mm)	3-4.5 /0.015	-	-
Tensile strength (Mpa)	1500-1700	377.64	17.2
Elastic modulus (Mpa)	72	18.7	2.72
Ultimate strain	-	0.00204	0.6322

Table 3. The characteristics of the GFRP

Proprieties	Specified Values	Number of Specified Values
fco	8.5; 16; 25 MPa	3
F	0.3; 0.6; 0.9; 1.2%	4
NL	2; 4; 6Layers	3
Total number 3x4x3=36 Specimens		

On the other hand, by paying particular attention to the cleaning and gluing of the fiber liners in order to optimize the confinement effects.

Table 3 shows the number of samples studied taking into account all the variables such as the compression concrete strength *fco*, the proportion of glass fibers in the concrete F and the number of confinement layers L.

For example, the sample S16-F0.3-NL4 has a *fco* = 16Mpa; F = 0.3%; NL = 4Layers.

2.2 Testing procedure

The evaluation methods for concrete reinforced by GFRP are essentially based on central compression tests to analyze the behavior of the material under axial loads. The test specimens were wrapped by a bidirectional sheath made of glass fibers and polyester resin of different thicknesses (t_f=0.4 mm for a single layer).

The samples undergo controlled axial compression using the UTS-SHIMADZU universal machine in accordance with the standard guidelines of ASTM D638 (2010) shown in Figure 1 with a capacity of 2000 kN and a constant travel speed of 0.1 KN /s; force and displacement sensors directly evaluate the applied stress and the deformation of the sample at an extremely fast sampling rate of up to 1 msec to accurately capture the moment of rupture.

This arrangement facilitates a progressive increase in the load while simultaneously capturing the responses of the samples in terms of deformation and stress (σ-ε). Throughout the test phase, data are collected at predetermined load increments in order to develop stress-strain curves. These curves shed light on crucial mechanical characteristics such as compressive strength, ductility and rigidity of GFRP compared to conventional concrete samples. Figure 2 shows a set of samples after the compression test.

Figure 1. The UTS-SHIMADZU universal machine

The information obtained from these experimental scenarios highlights the potential failure modes and highlights the improvements offered by fiber reinforcement. The completed tests have provided us with several results; the first result is that the glass fibers found in the concrete paste (F) have an obvious impact on the resistances of the concrete (*fc*); Table 4 presents the variation of the resistances of the concrete according to the rate of the fibers added and the type of concrete used design compared to ordinary concrete specimens.

Figure 2. Confined concrete specimens

Table 4. The variation in the strength of concrete according to the fiber content in the concrete

The Strength of Concrete According to the Rate of Glass Fibers F%				
0%	**0.3%**	**0.6%**	**0.9%**	**1.2%**
8.5Mpa	10.25 Mpa	11.68 Mpa	10.68 Mpa	9.35 Mpa
16Mpa	20.69 Mpa	21.12 Mpa	20.48 Mpa	17.9 Mpa
25Mpa	31.6 Mpa	33.01 Mpa	32.74 Mpa	27.5 Mpa

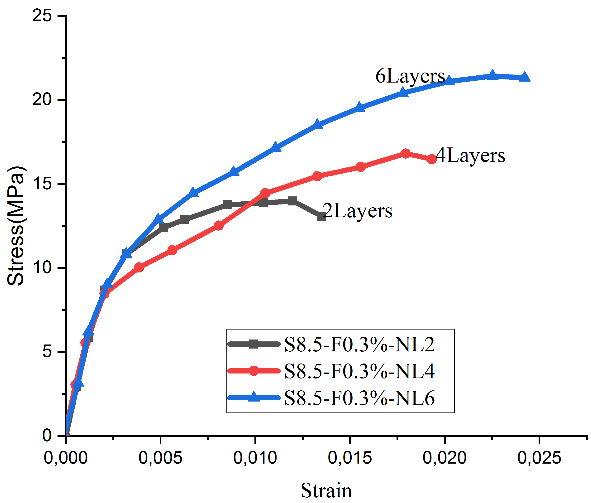

Figure 3. Variation of the confinement layers specimen of *fc* = 8.5Mpa and F = 0.3%

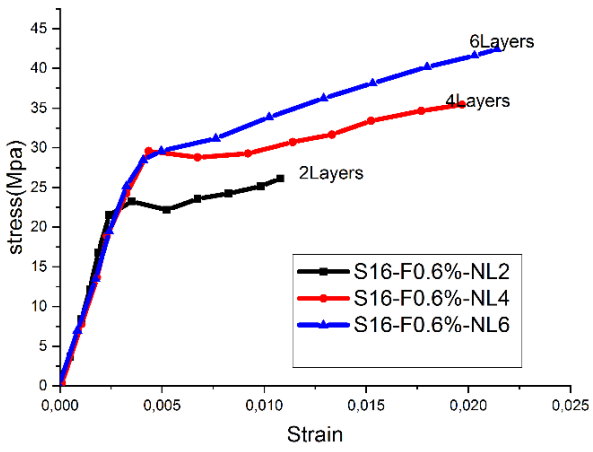

Figure 4. Variation of the confinement layers specimen of *fc* = 16MPa and F = 0.6%

In addition, curves of the behavior of compressed concrete have been drawn to demonstrate the effect of the variation in the number of confinement layers; the variation in strength and the variation in the glass fiber content on the stress–deformation rate; Figures 3–5 represent the effect of the variation in the number of layers for samples made for different strengths. The results obtained seem very logical awaiting confirmation in the next parts of this research.

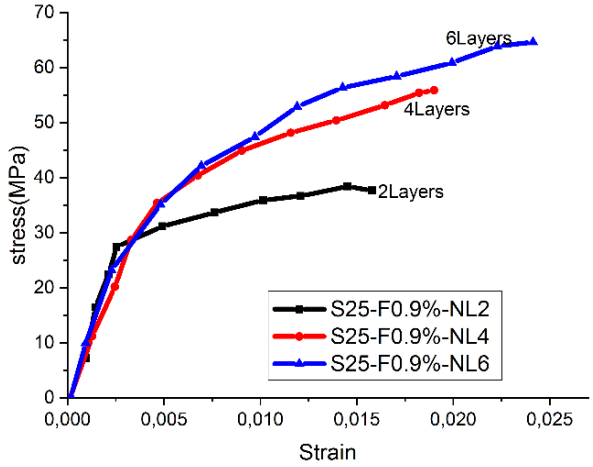

Figure 5. Variation of the confinement layers specimen of *fc* = 25 MPa and F = 0.9%

3. EXISTING STRESS-STRAIN MODELS OF FRP CONFINED CONCRETE

Various analytical models have been proposed in order to reproduce the behavior of stress (*fc*)-deformation (*εc*) law of a cylindrical concrete test piece wrapped externally with FRP composite sheets and subjected to axial compression; Table 4 contains six expressions concerning the laws of behavior including all the parameters related to it, the formulas are suggested by the studies [18-23].

4. COMPARISON BETWEEN THE EXPERIMENTAL RESULTS AND EXISTING MODELS

In order to verify the relevance of the tests that we have carried out, as well as the applicability of the behavioral laws suggested by the researchers and the extent of their effectiveness, an analytical study is carried out. The proposed numerical analysis is based on the determination of the relationship (σ-ε) in each slice of the cross section. The depth of the compressed zone being known (Xu) as well as: the diameter of the cylinder of the confined concrete D; The strength of the unconfined concrete strength *fco*; elastic modulus of FRP in the hoop direction E_f; thickness of FRP jacket (t_f) and ε_f: hoop rupture strain of the FRP jacket. *fl:* confinement pressure provided by the FRP jacket. *fcc*: resistance of confined concrete. Ec: elastic modulus of unconfined concrete (MPa); E2: Second slope of the stress-strain response; εc: axial stress; εt: peak axial deformation and εcu: ultimate axial deformation are calculated according to the expressions proposed by each author. The compressed area is divided into unit slices (X); For each slice, the torque (σ-ε) is obtained thus giving a point of the behavior curve. By doing an iteration in the section (X=0 to X=XU); and through the results all the points of the curve (σ-ε) are finally obtained. Indeed, six separate programs have been carefully developed, allowing us to calculate all the factors and parameters created

and developed by the six researchers mentioned in Table 5, while respecting the specificities of each proposed expression.

Figure 6 shows an example of the structure of the program for the study of the laws of Lam.

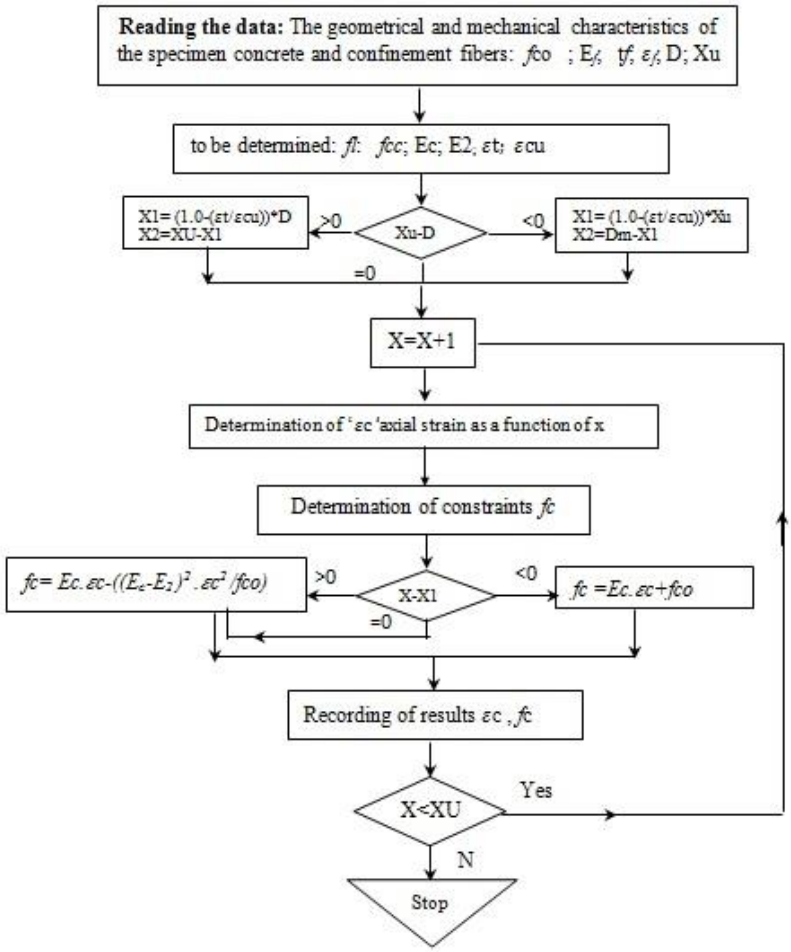

Figure 6. The structure of the program for the laws of Lam

Table 5. Stress-strain curve model

Laws of Behaviour	Expressions
Samaan et al. [18]	$f_c = \frac{(E_c-E_2)\varepsilon_c}{\left[1+\left(\frac{(E_c-E_2)}{fo}\right)^n\right]^{1/n}} + E_2\varepsilon_c \ldots\ldots 0 \le \varepsilon_c \le \varepsilon_{cu}$ $n=1.5;\ E_c = 3950\sqrt{fco}\ [MPa];\ f_{co}=f_{c28};\ E_2 = 245.61fco^{0.2} + 1.3456\frac{E_f.t_f}{D}[Mpa];\ f_l = \frac{2.E_f.\varepsilon_f.t_f}{D};\ fcu = fco + 6.0fl^{0.7}\ [MPa];\ \varepsilon_{cu} = \frac{fcu-fo}{E_2};\ fo = 0.872fco + 0.371fl + 6.258\ [MPa]$
Lam and Teng [19]	$f_c = E_c\varepsilon_c - \frac{(E_c-E_2)^2}{fco}\varepsilon_c{}^2 \ldots\ldots\ldots if\ 0 \le \varepsilon c \le \varepsilon t$ $f_c = E_2\varepsilon_c + fco \ldots\ldots\ldots if\ \varepsilon t \le \varepsilon c \le \varepsilon_{cu}$ $E_c = 4730\sqrt{fco}\ [Mpa];\ \varepsilon_t = \frac{2fco}{E_c-E_2};\ E_2 = \left(\frac{fcc-fco}{\varepsilon_{cu}}\right);\ fl = \frac{2E_f.t_f.\varepsilon_f}{D};\ \frac{\varepsilon_{cu}}{\varepsilon_{c0}} = 1.75 + 12\left(\frac{fl}{fco}\right)\left(\frac{\varepsilon_f}{\varepsilon co}\right)^{0.45};\ \varepsilon_{c0} = 0.002;$ $\frac{fcc}{fco} = 1 + 3.3\left(\frac{fl}{fco}\right) \ldots\ldots\ldots if\ \frac{f_l}{fco} \ge 0.07;\ \frac{fcc}{fco} = 1 \ldots\ldots\ldots if\ \frac{f_l}{fco} < 0.07$
Jiang and Teng [21]	$fc = \left(\frac{(\varepsilon c/\varepsilon cc)r}{r-1+(\varepsilon c/\varepsilon cc)^r}\right)fcc$ $r = \left(\frac{Ec}{Ec-\left(\frac{fcc}{\varepsilon cc}\right)}\right);\ E_c = 4730\sqrt{fco}\ [Mpa];\ \frac{fcc}{fco} = 1 + 3.5\frac{fl}{fco};\ \frac{\varepsilon cc}{\varepsilon co} = 1 + 17.5(\frac{fl}{fco'})^{1.2};\ \varepsilon_{c0} = 0.00937\sqrt{fco};\ fl = \frac{2.E_f.t_f.\varepsilon_f}{D}.$
Youssef et al. [20]	$for\ 0 \le \varepsilon c \le \varepsilon t: f_c = Ec.\varepsilon c\left[1 - \frac{1}{n}\left(\left(\frac{\varepsilon c}{\varepsilon t}\right)^{n-1}\right)\right];\ n = \frac{Ec.\varepsilon t}{Ec.\varepsilon t - ft} \ldots\ldots\ldots if\ E_2 < 0$ $fc = Ec.\varepsilon c\left[1 - \frac{1}{n}\left(1 - \frac{E2}{Ec}\right)\left(\frac{\varepsilon c}{\varepsilon t}\right)^{n-1}\right];\ n = \frac{(Ec-E2).\varepsilon t}{Ec.\varepsilon t - ft} \ldots\ldots\ldots if\ E_2 > 0$ $For\ \varepsilon t \le \varepsilon c \le \varepsilon_{cu}: f_{co} = ft + E2(\varepsilon c - \varepsilon t).$ $E_c = 4730\sqrt{fco}[Mpa];\ \rho f = \frac{4.t_f}{D};\ fju = E_f.\varepsilon_f;\ fl = \frac{1}{2}.\rho_f.fju;\ fcu = fco(1 + 2.25(\frac{fl}{fc})^{5/4}\ [Mpa];$ $\varepsilon cu = 0.003368 + 0.259\left(\frac{flu}{fco}\right)(\frac{fju}{Ef})^{1.2};\ ft = fco(1 + 3(\frac{\rho_f.E_f.\varepsilon f}{fco})^{5/4}.;\ \varepsilon t = 0.002748 + 0.1169(\frac{\rho_f.E_f.\varepsilon_f}{fco})^{6/7}(\frac{fju}{Ef})^{1/2};$ $E_2 = \left(\frac{fcu-ft}{\varepsilon_{cu}-\varepsilon t}\right)$

	$fc = \frac{fc1(\varepsilon c/\varepsilon c1)n}{n-1+(\varepsilon c/\varepsilon c1)^n} \ldots\ldots\ldots\ldots if\ 0 \le \varepsilon c \le \varepsilon c_1$
	$fc = fc1 + E_2(\varepsilon_c - \varepsilon_{c1}) \ldots\ldots if\ \varepsilon c_1 \le \varepsilon c \le \varepsilon cu$
Pour et al. [23]	$n = \left(\frac{Ec}{Ec - \frac{fc1}{\varepsilon c1}}\right);\ E_c = 4730\sqrt{fco}\ [Mpa];\ fl = \left(\frac{2E_f.t_f.\varepsilon_f}{D}\right);\ Kl = \left(\frac{2E_f.t_f}{D}\right);\ fcc = fco + k_1.K_l.\varepsilon_{fu}$
	$k_1 = 2.5 - 0.01fco;\ k_2 = 0.3 - 0.001fco;\ \varepsilon_{cO} = \frac{fco^{0.225}}{1000}(\frac{152}{D})^{0.1}(\frac{2D}{H})^{0.13}; \varepsilon_{cu} = 1.5\varepsilon_{co} + k_2\left(\frac{K_l}{fco}\right)^{0.75}(\varepsilon_f)^{1.35};$
	$f_{c1} = fco + 0.07.K1;\ \varepsilon c1 = \varepsilon_{cO}\left(1 + 0.024\frac{K1}{fco}\right);\ E_2 = \left(\frac{fcc - fc1}{\varepsilon_{cu} - \varepsilon_{c1}}\right).$
	$f_c = E_c\varepsilon_c - \frac{(E_c - E_2)^2}{4fco} \ldots\ldots\ldots if\ 0 \le \varepsilon c \le \varepsilon t$
	$f_c = fco + E_2\varepsilon_c \ldots\ldots\ldots\ldots\ldots if\ \rho_K \ge 0.01$
	$f_c = fco - \frac{fcc - fco}{\varepsilon_{cu} - \varepsilon_{cO}}(\varepsilon_c - \varepsilon_{c0}) \ldots if\ \varepsilon t \le \varepsilon c \le \varepsilon_{cu}$
Teng et al. [22]	$E_c = 4730\sqrt{fco}\ [Mpa];\ \varepsilon_{c0} = 9.37.10^{-4}.\sqrt[4]{fco} \ldots\ldots \varepsilon_{c0} > 0.002;\ \rho_K = \frac{2E_f t_f}{(\frac{fco'}{\varepsilon_{co}})D}\ and\ \rho_\varepsilon = \frac{\varepsilon_f}{\varepsilon_{co}};\ \frac{\varepsilon_{cu}}{\varepsilon_{co}} = 1.75 + 6.5.\rho_K{}^{0.8}.\rho_\varepsilon{}^{1.45}$
	$\frac{fcc}{fco} = 1 + 3.5(\rho_K - 0.01)\rho_\varepsilon \ldots\ldots if\ \rho_K \ge 0.01$
	$\frac{fcc}{fco} = 1 \ldots\ldots\ldots if\ \rho_K < 0.01$
	$E_2 = \left(\frac{fcc - fco}{\varepsilon_{cu}}\right)\ and\ \varepsilon_f = \frac{2fco}{E_c - E_2}$

The illustrations present experimental plots of σ-ε for circular samples surrounded by a GRFP sheath, compared to curves of σ-ε elaborated according to the models suggested by the studies [18-23]. It is emphasized that all the expressions suggested by the researchers examine samples of ordinary concrete confined by polymer composites, while our tests are carried out on GRFP confined concrete which also contains glass fibers; the strengths considered in this comparison are those obtained following the tests presented in Table 4.

4.1 The experimental results vs the Samaan model

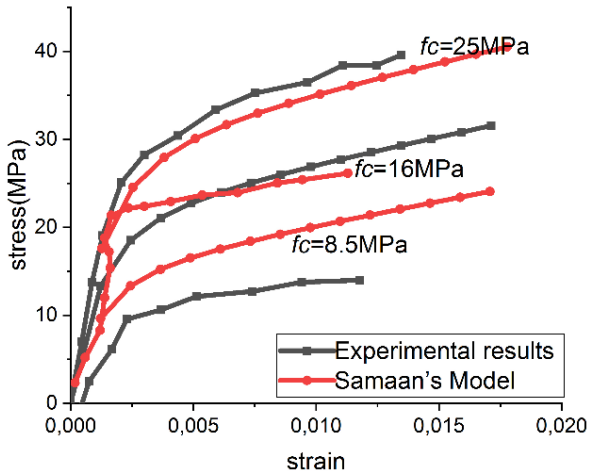

Figure 7. Comparison of stress-strain curves between experimental results and Samaan's model (F0.3%-NL2)

The following curves present the comparison between the experimental data and the data of Samaan et al. [18] analytical model which shows an important accuracy depending on the strength of the concrete in Figure 7, and the number of confinement layers in Figure 8. For *fc* = 25 MPa, the analytical model demonstrates an excellent agreement with the experimental results, showing deviations of only 5 to 8% over the entire deformation range and accurately predicting the maximum stress and post-peak behavior. At *fc* = 16 MPa, the model maintains a reasonable accuracy with an underestimation of about 10 to 15% of the peak values while preserving the overall characteristics of the curve. However, for *fc* = 8.5 MPa, significant deviations appear, the analytical model underestimating the experimental peak stress by 20 to 25% and showing a reduced accuracy in the post-peak prediction.

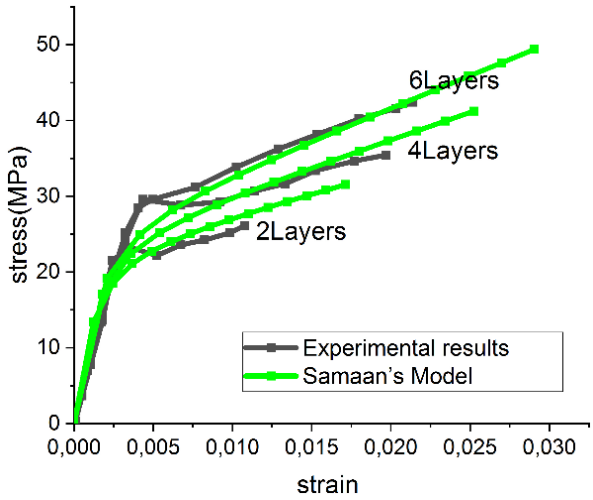

Figure 8. Comparison of stress-strain curves between experimental results and Samaan's model(S16-F0.6%)

4.2 The experimental results vs the Pour model

Figure 9 presents the comparison between the experimental data and the analytical model of Pour et al. [23], which reveals contrasting performances according to the strength of the concrete. For *fc* = 8.5 MPa, the analytical model shows a good agreement with the experimental results, with deviations generally between 8 and 12% for the maximum stress values and a reasonable correlation in the post-peak region. At *fc* = 16 MPa, the model demonstrates an improved accuracy with a difference of about 5 to 10% compared to the experimental values, in particular for the capture of the maximum stress and the initial behavior of softening by deformation. However, for *fc* = 25 MPa, the Pour model has a significant overestimation of the experimental maximum stress of about 15 to 20%, showing less conservative predictions compared to concrete of lower strength. The results indicate that the analytical model of Pour et al. [23] with the specified parameters provides a variable accuracy that does not follow a trend consistent with the strength of the concrete, working best at moderate strength

levels (*fc=16 MPa*) and also if the number of confinement layers is high in Figure 10; but showing increased deviations at lower and upper resistance ranges with a low number of confinement layers, suggesting the need for resistance-dependent calibration factors for optimal prediction accuracy.

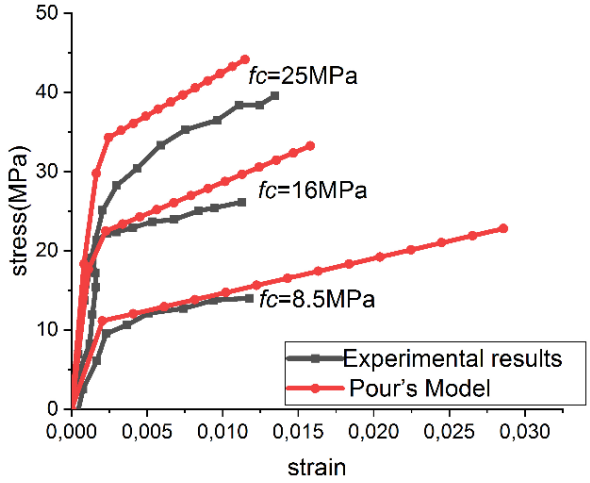

Figure 9. Comparison of stress-strain curves between experimental results and Pour's model (NL2- F0.3%)

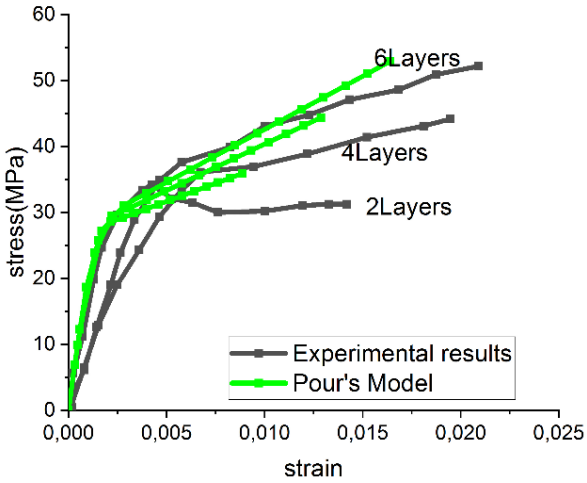

Figure 10. Comparison of stress-strain curves between experimental results and Pour's model (S25-F1.2%)

4.3 The experimental results vs the Teng model

A comparison between the experimental data and the analytical model of Teng et al. [22] (Figure 11) demonstrates a good constant agreement for all levels of strength of concrete as well as the variation concerning the number of confinement layers. For *fc = 8.5 MPa*, the analytical model shows an excellent correlation with the experimental results, with deviations of about 3 to 7% in the prediction of the maximum stress and an accurate representation of the softening behavior after the peak. At *fc = 16 MPa*, the model maintains high accuracy with differences generally between 5 and 10% of the experimental values, effectively capturing the ascending and descending parts of the stress-strain curve. For *fc = 25 MPa*, the Teng model continues to work well with maximum stress predictions between 8 and 12% of the experimental data, although it slightly overestimates the ultimate deformation capacity with the increase in the number of layers in Figure 12. This model demonstrates superior performance in capturing the behavior of confined concrete regardless of the strength level and the number of layers, making it a robust choice for engineering applications involving fiber-reinforced concrete containment systems.

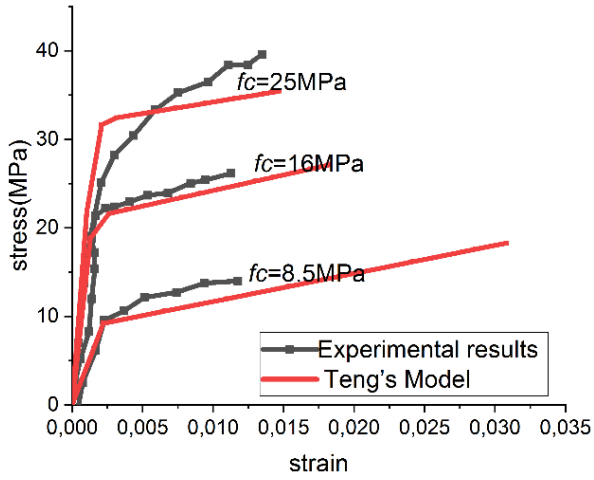

Figure 11. Comparison of stress-strain curves between experimental results and Teng's model (NL2-F0.3%)

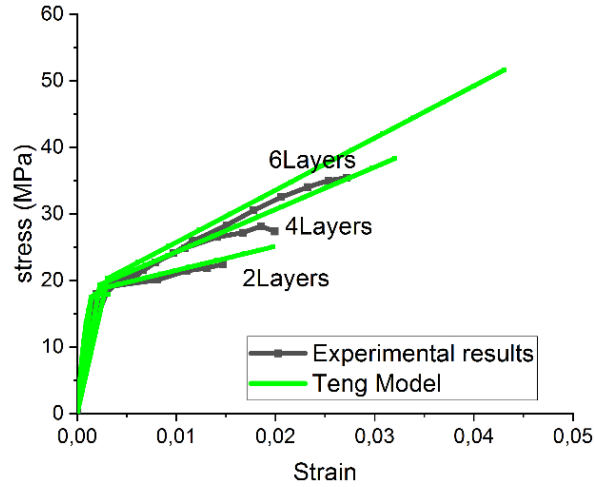

Figure 12. Comparison of stress-strain curves between experimental results and Teng's model (S16-F0.9%)

4.4 The experimental results vs the Lam model

The comparison between the experimental data and the analytical model of Lam and Teng [19] shows a concordance on all levels of concrete strength with remarkable consistency. For *fc* = 25 MPa, the analytical model demonstrates moderate accuracy with deviations of only 2 to 5% from the experimental peak stress values and an accurate prediction of the complete stress-strain behavior, including post-peak softening in Figure 13. At *fc* = 16 MPa, the model maintains exceptional performance with differences generally between 3 and 7% compared to experimental results, accurately capturing both the rigidity of the ascending branch and the softening characteristics under stress. For *fc* = 8.5 MPa, the Lam model continues to show a superior correlation with the experimental data; including the post-peak softening, an overestimation of the peak stress is clear while effectively modeling the post-peak behavior and the ultimate deformation capacity. For this model, the variation in the number of layers has a weak effect compared to other models in Figure 14.

However the results demonstrate that Lam's analytical model provides reliable and consistent predictions; it is among the best models compared, with an accuracy of 8% over the entire resistance range of concrete.

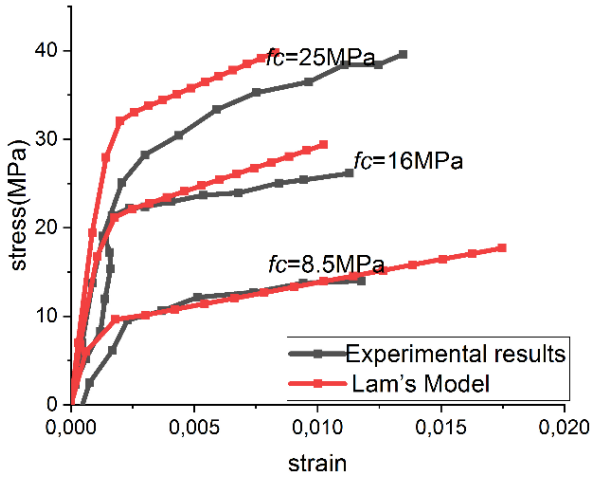

Figure 13. Comparison of stress-strain curves between experimental results and Lam's model Lam (NL2-F 0.3%)

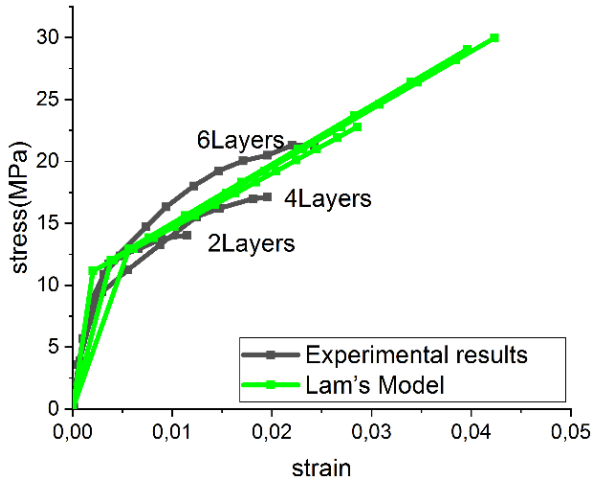

Figure 14. Comparison of stress-strain curves between experimental results and Lam's model S8.5-F0.3%

4.5 The experimental results vs the Jiang model

The comparison between the experimental data and the analytical model of Jiang and Teng [21] shows variable performances according to the different levels of resistance of the concrete shown in Figure 15. For *fc* = 25 MPa, the analytical model demonstrates a very reasonable agreement with the experimental results, showing deviations of about 10 to 15% in the prediction of the peak stress while adequately capturing the general shape of the stress-strain curve and the behavior after the peak. At *fc* = 16 MPa, the model retains moderate accuracy with differences generally between 12 and 18% of the experimental values, although it tends to slightly overestimate the peak stress and shows a certain deviation in the region of stress softening. For fc = 8.5 MPa, the Jiang model presents more significant deviations with an overestimation of the experimental peak stress of about 15 to 20%. The results indicate that Jiang's analytical model offers moderate accuracy, with a tendency to overestimate the strength of confined concrete, especially at low strength levels; the curves in Figure 16 prove this once again. Although the model captures the fundamental behavior of confinement, its accuracy is lower than that of other analytical approaches, with prediction errors ranging from 10 to 20% for the tested concrete strengths, which suggests the need to adjust the calibration to improve accuracy in engineering applications.

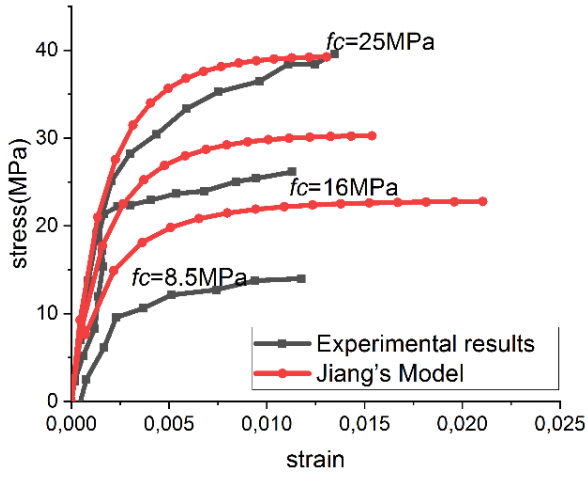

Figure 15. Comparison of stress-strain curves between experimental results and Jiang's model (NL2-F 0.3%)

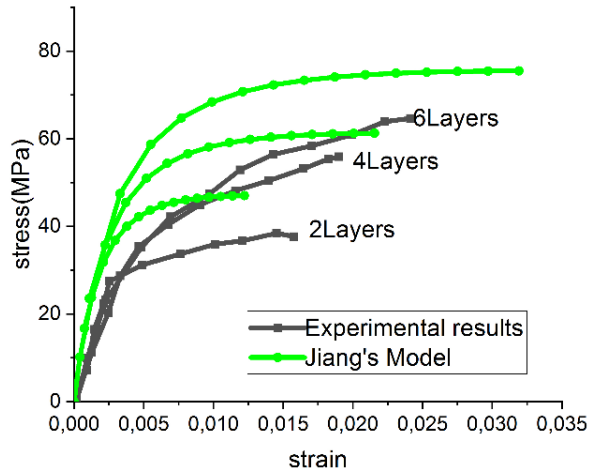

Figure 16. Comparison of stress-strain curves between experimental results and Jiang's model S25-F0.9%

4.6 The experimental results vs the Youssef model

Figure 17 presents the comparison between the experimental data and the analytical model of Youssef et al. [20], which reveals significant differences for all levels of strength of concrete. For *fc* = 8.5 MPa, the analytical model shows a substantial overestimation of the experimental results with deviations of about 25 to 35% in the prediction of the maximum stress, while presenting different curve characteristics with a more pronounced work hardening behavior than that observed experimentally. At *fc* = 16 MPa, the model continues to significantly overestimate the strength of the confined concrete by 30 to 40%, the analytical curve showing a markedly different shape which includes a plateau region absent from the experimental data. For *fc* = 25 MPa shown in Figure 18, Youssef's [20] model shows the largest deviations with an overestimation of the experimental maximum stress of 40 to 50%, displaying an unrealistic stress-

strain relationship that includes large stress drops and subsequent increases that contradict the experimental observations.

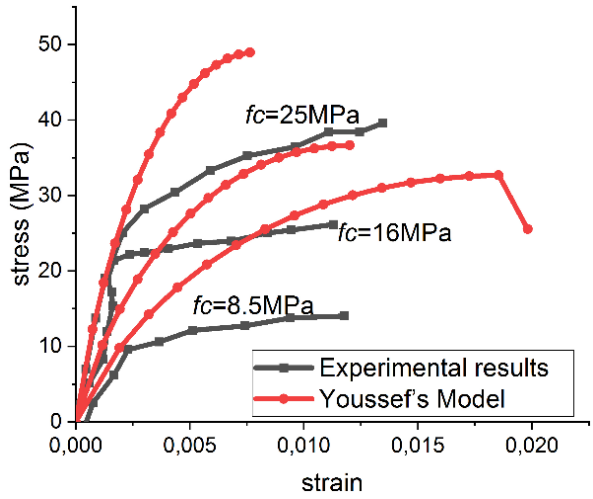

Figure 17. Comparison of stress-strain curves between experimental results and Youssef's model NL2-F0.3%

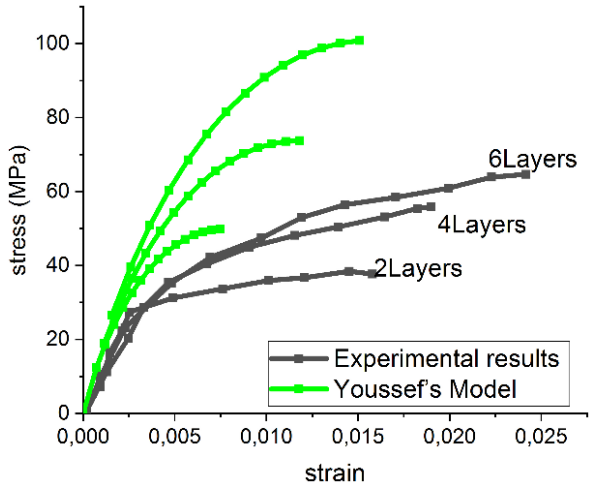

Figure 18. Comparison of stress-strain curves between Experimental results and Youssef's model S25-F=0.9%

The results indicate that Youssef's analytical model, with the parameters used, has a low correlation with the experimental data for all the concrete strengths tested, systematically overestimating the capacity of the confined concrete and exhibiting unrealistic behaviors.

This model has the lowest accuracy among all the analytical approaches compared, with prediction errors between 25 and 50%, which makes it unsuitable for reliable engineering design applications without recalibration or significant modification of the parameters.

5. RESULTS

The accuracy of each model to predict the ultimate resistance was quantified by calculating relative errors as a representative of the quality of the fit for each sample. The relative error as well as the average percentage of errors of the specimens of each group is presented in Tables 6 and 7.

The comparative analysis reveals significant variations in the accuracy and reliability of the model.

Pour et al.'s [23] model demonstrated exceptional performance for all concrete strengths, maintaining prediction errors between (0.3% and 27%) with an underestimate equal to 3.4%.

Samaan et al.'s [18] model showed a strength-dependent accuracy, with excellent performances for normal strength concrete (errors of 0. 9 % to 13% at fc = 25 MPa), but becoming more and more cautious for the lowest strengths (errors of 23% to 45%).

Teng et al. [22] model has a superior ability to capture the fundamental mechanics of the behavior of fiber-reinforced concrete, which makes it particularly suitable for engineering design applications requiring an accurate prediction of the response of confined concrete, regardless of its strength level.

It provides the most reliable and consistent predictions among all the models compared, with an exceptional accuracy of 6.4% over the entire resistance range of the concrete.

The model by Lam and Teng [19] showed variable performance without consistent trends, reaching optimal accuracy at moderate resistance levels (deviation of 0.8 to 19% at fc = 25 MPa) but displaying increased errors both in the low resistance ranges (23.3 to 38.5%) and higher (overestimation of 11.4%). The model by Jiang and Teng [21] provided moderate accuracy with a constant tendency to overestimate the strength of confined concrete, showing prediction errors ranging from 0.92% to 42.8% for all the tested strengths. The model of Youssef et al. [20] demonstrated the most mediocre performance, presenting a substantial overestimation (39.5%) and unrealistic behavior models that contradict experimental observations. Figure 19 represents the deviation of strengths relative to the experimental values; it is noted here that the values of the Youssef et al. [20] model are the most dispersed.

Table 6. The values of the ultimate compressive strengths

Fcu (MPa) / Specimens	Exp Results	Samaan Model	Teng Model	Pour Model	Jiang Model	Lam Model	Youssef Model
S8.5-F0.3-L2	14	25.82	19.48	19.38	24.5	22.76	33.30
S16-F0.6-L4	35.44	46.35	40.73	38.52	49.62	46.21	66.87
S25-F0.9-L2	39.6	40.5	30.35	33.4	39.24	37.54	49.95
S25-F0.9-L4	50.7	50.24	43.66	42.08	53.5	50.09	73.79
S25-F0.3-L6	61.02	56.33	61.53	61.57	63.65	61.53	100.26
S25-F0.6-L6	65.25	66.44	63.14	57.7	75.76	70.76	100.91
S25-F0.9-L6	64.63	66.17	62.93	57.48	75.49	70.73	100.78
S25-F1.2-L6	52.71	60.92	58.88	52.87	70.26	65.14	98.65

Table 7. Percentage error of the ultimate compressive strengths

Specimen Group	Samaan Model	Teng Model	Pour Model	Jiang Model	LamModel	Youssef Model
S8.5-F0.3-L2	+45	+28	+27.7	+42.8	+38.5	+60
S16-F0.6-L4	+23.5	+13	+8	+28 .5	+23.3	+47
S25-F0.9-L2	+2.2	-30.5	-18.5	-0.92	-5.5	+20.7
S25-F0.9-L4	-0.9	-16.1	-20.5	+5.2	-1.2	+31.3
S25-F0.3-L6	-8.3	+0.8	+0.9	+4.1	+0.8	+39.1
S25-F0.6-L6	+1.8	-3.3	-13	+13.8	+7.8	+35.3
S25-F0.9-L6	+2.3	2.7	-12.4	+14.4	+8.6	+35.9
S25-F1.2-L6	+13.5	+10.4	+0.3	+25	+19	+46.5
Mean	**+9%**	**+6.4%**	**-3.4%**	**+16.6%**	**+11.4%**	**+39.5%**

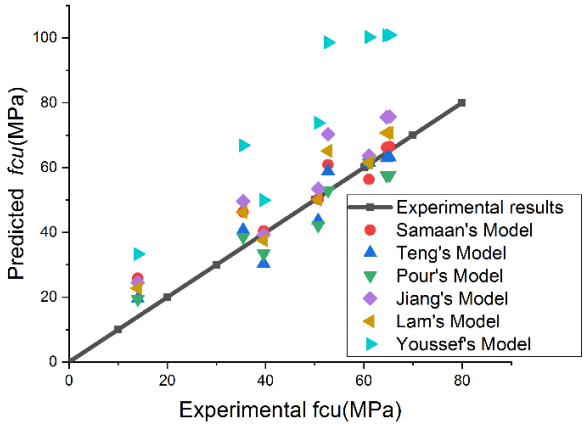

Figure 19. Ultimate strengths *fcu* predicted by selected models versus test results

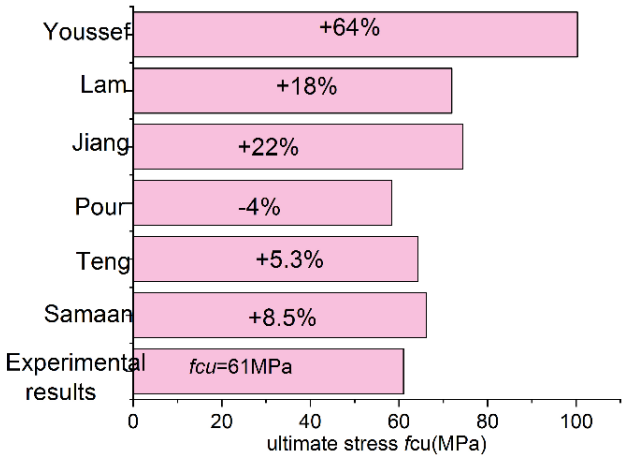

(a) Ultimate strength predictions

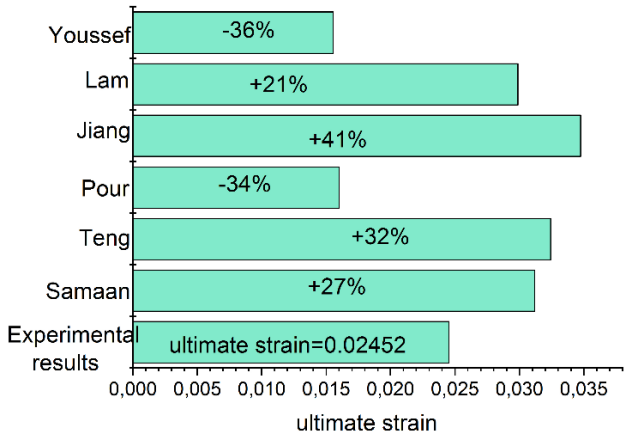

(b) Ultimate strain predictions

Figure 20. Performance of the existing models and experimental results

To comprehensively compare the models, their ability to predict the ultimate strength and deformation is also evaluated; accordingly, the percentages of the errors of each model in the prediction of the ultimate strength and deformation samples are presented in Figure 20, the data represent the errors for the same sample the same results were predicted by the models, the Pour et al.'s model [23] provided the most accurate prediction of the ultimate resistance as well as the deformation; given its average errors lower by 4% compared to the resulting errors of the other models, all the models presented the same order of average error for the ultimate resistances, indicating their similar accuracy in predicting the ultimate deformation.

6. CONCLUSION

This study presents an evaluation of six analytical models making it possible to predict the stress-deformation behavior of fiber-reinforced confined concrete, by comparing them with experimental data. The analysis focused on concrete strengths ranging from 8.5 to 25 MPa with consistent fiber parameters (thickness e = 0.8 to 2.4 mm, fiber content W = 0.3 to 1.2%). Experimental tests were envisaged and compared by the six analytical models to predict the real stress-strain and at the same time evaluate the reliability of the six analytical models. The evaluation of analytical models for fiber-reinforced confined concrete reveals crucial information for engineering practice and future research directions. Among the tested models, Pour et al.'s [23] model stands out as the most reliable and accurate, systematically capturing the basic mechanics of containment and proving to be perfectly adapted to practical technical design. Conversely, the notable discrepancies in the Youssef et al. [20] model highlight the critical need for rigorous validation of experimental data before adopting any analytical model for design purposes. These findings underscore that not all existing analytical formulations offer the precision required for practical applications, highlighting a gap that future research must address. Advancing model accuracy across varying concrete strengths and fiber configurations remains essential, with promising avenues including the integration of machine learning techniques and advanced constituent modeling. Such innovations hold the potential to deepen our understanding of the complex behavior inherent in confined fiber-reinforced concrete systems, ultimately leading to more robust and reliable design tools for engineering practice.

REFERENCES

[1] Xiao, Y., Wu, H. (2000). Compressive behavior of concrete confined by carbon fiber composite jackets. Journal of Materials in Civil Engineering, 12(2): 139-146.

https://doi.org/10.1061/(ASCE)0899-1561(2000)12:2(139)
[2] Zohrevand, P., Mirmiran, A. (2013). Stress-strain model of ultrahigh performance concrete confined by fiber-reinforced polymers. Journal of Materials in Civil Engineering, 25(12): 1822-1829. https://doi.org/10.1061/(ASCE)MT.1943-5533.0000769
[3] Wang, M., Zheng, Y.F. (2025). A decision-oriented modelling framework for sustainable strengthening of reinforced concrete structures using data-driven capacity prediction. Mathematical Modelling for Sustainable Engineering, 1(2): 94-101. https://doi.org/10.56578/mmse010203
[4] Yang, J., Wang, J., Wang, Z. (2020). Axial compressive behavior of partially CFRP confined seawater sea-sand concrete in circular columns–Part II: A new analysis-oriented model. Composite Structures, 246: 112368. https://doi.org/10.1016/j.compstruct.2020.112368
[5] Piancastelli, L., Lorenzini, E. (2025). Innovating modern cement by harnessing solutions from ancient Roman concrete. Journal of Civil and Hydraulic Engineering, 3(3): 151-158. https://doi.org/10.56578/jche030303
[6] Isleem, H.F., Peng, F., Tayeh, B.A. (2022). Confinement model for LRS FRP-confined concrete using conventional regression and artificial neural network techniques. Composite Structures, 279: 114779. https://doi.org/10.1016/j.compstruct.2021.114779
[7] Babba, R., Douadi, A., Alsuhaibani, E., Moretti, L., Merdas, A., Dahmani, S., Boutlikht, M. (2025). The impact of confinement configurations on the compressive behavior of CFRP—wrapped concrete cylinders. Materials, 18(15): 3559. https://doi.org/10.3390/ma18153559
[8] Dahmani, S., Khitas, N.E.H., Babba, R., Hebbache, K., et al. (2025). Carbon Fiber-Reinforced Polymer (CFRP) confinement strategies for concrete columns: Evaluating the efficacy of full and partial wrapping methods. Metallurgical and Materials Engineering, 31(3): 238-246. https://doi.org/10.63278/1361
[9] Minafò, G., Papia, M. (2016). Concrete softening effects on the axial capacity of RC jacketed circular columns. Engineering Structures, 128: 215-224. https://doi.org/10.1016/j.engstruct.2016.09.043
[10] Cao, Y.G., Jiang, C., Wu, Y.F. (2016). Cross-sectional unification on the stress-strain model of concrete subjected to high passive confinement by fiber-reinforced polymer. Polymers, 8(5): 186. https://doi.org/1.3390/polym8050186
[11] Ribeiro, F., Sena-Cruz, J., Branco, F.G., Júlio, E. (2018). Hybrid FRP jacketing for enhanced confinement of circular concrete columns in compression. Construction and Building Materials, 184: 681-704. https://doi.org/10.1016/j.conbuildmat.2018.06.229
[12] Limaiem, M., Ghorbel, E., Limam, O. (2019). Comparative experimental study of concrete reparation with carbon epoxy & bio-resourced composites. Construction and Building Materials, 210: 312-323. https://doi.org/10.1016/j.conbuildmat.2019.03.137
[13] Zhu, Z., Zhou, Y., Li, Z., Li, H., Hu, B., Li, P. (2022). A versatile continuous model for predicting various post-peak patterns of FRP-confined concrete. Composite Structures, 294: 115750. https://doi.org/10.1016/j.compstruct.2022.115750
[14] Hamzaoui, L., Bouzid, T. (2021). The proposition of an EI equation of square and L–shaped slender reinforced concrete columns under combined loading. Engineering, Technology & Applied Science Research, 11(3): 7100-7106. https://doi.org/10.48084/etasr.4048
[15] Djarir, Y., Belgacem, M., Mohamed, S., Tayeb, B. (2022). Experimental verification of the new models applied to glass fibre reinforced concrete (GFRC) confined with glass fibre reinforced polymer (GFRP) composites. Ceramics Silikaty, 66(3): 384-395. https://doi.org/10.13168/cs.2022.0034
[16] Zendaoui, A., Saadi, M., Yahiaoui, D., Amouri, C. (2024). An experimental and analytical study on the compressive behavior of glass fiber reinforced concrete (GFRC) confined with GFRP composites. Engineering, Technology & Applied Science Research, 14(6): 17939-17944. https://doi.org/10.48084/etasr.8750
[17] Yahiaoui, D., Saadi, M., Bouzid, T. (2022). Compressive behavior of concrete containing glass fibers and confined with glass FRP composites. International Journal of Concrete Structures and Materials, 16(1): 37. https://doi.org/10.1186/s40069-022-00525-9
[18] Samaan, M., Mirmiran, A., Shahawy, M. (1998). Model of concrete confined by fiber composites. Journal of Structural Engineering, 124(9): 1025-1031. https://doi.org/10.1061/(ASCE)0733-9445(1998)124:9(1025)
[19] Lam, L., Teng, J.G. (2003). Design-oriented stress–strain model for FRP-confined concrete. Construction and Building Materials, 17(6-7): 471-489. https://doi.org/10.1016/S0950-0618(03)00045-X
[20] Youssef, M.N., Feng, M.Q., Mosallam, A.S. (2007). Stress–strain model for concrete confined by FRP composites. Composites Part B: Engineering, 38(5-6): 614-628. https://doi.org/10.1016/j.compositesb.2006.07.020
[21] Jiang, T., Teng, J.G. (2007). Analysis-oriented stress–strain models for FRP–confined concrete. Engineering Structures, 29(11): 2968-2986. https://doi.org/10.1016/j.engstruct.2007.01.010
[22] Teng, J.G., Jiang, T., Lam, L., Luo, Y.Z. (2009). Refinement of a design-oriented stress–strain model for FRP-confined concrete. Journal of Composites for Construction, 13(4): 269-278. https://doi.org/10.1061/(ASCE)CC.1943-5614.0000012
[23] Pour, A.F., Ozbakkaloglu, T., Vincent, T. (2018). Simplified design-oriented axial stress-strain model for FRP-confined normal-and high-strength concrete. Engineering Structures, 175: 501-516. https://doi.org/10.1016/j.engstruct.2018.07.099

NOMENCLATURE

FRP	Fiber Reinforced Polymer.
GFRP	Glass Fiber Reinforced Polymer.
S	Sample

Greek symbols

σ	Constraint
ρ_f	The volumetric ratio of FPR jacket.
ρ_k	Confinement stiffness ratio.
ρ_ε	Confinement strain ratio.

ε_c	Axial strain in concrete.
ε_{cc}	Strain in concrete at peak confined stress.
ε_{co}	Peak strain of unconfined concrete.
ε_{cu}	Ultimate axial strain of confined concrete.
ε_j	Ultimate strain of the FRP jacket.
ε_t	Peak strain of confined concrete.

Subscripts

D	Diameter of circular specimen.
E_c	Initial tangent modulus of concrete.
Ej	Modulus of elasticity of jacket in hoop.
F	Rate of glass fibers in concrete.
f_c	Concrete compressive strength.
fc_{28}	Compressive strength at 28 days.
fcc	Compressive strength of confined concrete.
fco	Compressive strength of unconfined concrete.
fcu	Ultimate compressive stress of confined concrete.
fju	Tensile strength of the FRP jacket.
fl	Hoop tensile strength of the FRP jacket.
ft	Peak stress of confined concrete.
K	Slope of the fitted straight line.
K_1	Parameter function of *fco*
K_2	Parameter function of *fco.*
tf	Thickness per layer of FRP jacket.